Bull. Mater. Sci., Vol. 34, No. 3, June 2011, pp. 499–506. © Indian Academy of Sciences.

Electronic properties and charge density of $Be_xZn_{1-x}Te$ alloys

C B SWARNKAR[†], U PALIWAL, N N PATEL[‡] and K B JOSHI[*]
Department of Physics, M.L. Sukhadia University, Udaipur 313 001, India
[†]Department of Physics, S.G.G. Govt. (PG) College, Banswara 327 001, India

MS received 7 August 2010; revised 14 November 2010

Abstract. Electronic band structure calculations are performed for the $Be_xZn_{1-x}Te$ ($0 \leq x \leq 1$ in steps of 0·2) alloys following the empirical pseudopotential method. The alloying effects are modelled through the modified virtual crystal approximation. Throughout the composition, valence band maximum resides at the Γ point. The conduction band minimum, however, shifts from Γ to *X* point of symmetry when $x = 0{\cdot}27$. The observed crossover from direct to indirect bandgap is well in accordance with the experimental observations. Effect of alloying on the density of states is also discussed. The charge density distribution along a few major planes is computed and discussed. The electronic band structure related parameters like bandwidths, bandgaps and ionicity are reported and compared with experimental data wherever available. We also give estimates of cohesive energy and bulk modulus for the alloys.

Keywords. II–VI semiconductor alloys; band structure; charge density; empirical pseudopotential method.

1. Introduction

II–VI semiconductors have technological applications in fabricating optoelectronic devices, detecting systems for environmental pollution, and colour displaying modules (Dhamani *et al* 1993). Structural quality, ohmic contacts, band offsets and device degradation pose serious problems in our attempts of enhancing performance of these devices (Fan *et al* 1992; Dhamani *et al* 1993; Waag *et al* 1996; Berghout *et al* 2007; Adachi 2009). In search of credible alternatives to improve performance of optoelectronic devices by minimizing the contact potentials and reduce the lattice mismatch etc cationic and anionic alloys from the III–V and II–VI families of semiconducting alloys are being tried. Possibilities of controlling physical properties of these alloys in the entire range of composition offer immense scope and advantage.

BeTe alloying with ZnTe could offer the opportunity to create new family of wide bandgap semiconductors (Verie 1997; Niiyama and Watanabe 2005). Essentially hardness, lattice matching, high *p*-type doping, better surface morphology (Kishino and Nomura 2002), together with different types of bonding in BeTe and ZnTe have caused resurgence of interest in these alloys (Waag *et al* 1997). $Be_xZn_{1-x}Te$ is a novel alloy system and used in injected laser diodes at 560 nm (Che *et al* 2002). It has been observed to be difficult to obtain lasing emission at this wavelength from other laser diodes from quaternary alloys of phosphides and or nitrides of Al, Ga and In (Nakamura *et al* 2000). Moreover, direct bandgap in these alloys enables its use as transparent conductive electrode in solar cells and photo-detectors (Maksimov *et al* 2004). Furthermore, the alloys at $x = 0{\cdot}94$, 0·91, 0·48 and 0·10 have lattice matching with GaAs, ZnSe, InP and InAs, respectively.

For binary beryllium chalcogenides first-principles calculations are performed to report bulk modulus and electronic band structure (Stukel 1970; Gonzalez-Diaz *et al* 1997; Verie 1997; Kalpana *et al* 1998; Nagelstraβer *et al* 1998; Srivastava *et al* 2004). These calculations predicted higher covalent character of bonding compared to other wide gap II–VI semiconductors like ZnTe. The first-principles methods give diverging estimates of bandgaps in semiconductor compounds (Cohen 2006). However, better estimates in binary semiconductors are obtained when Hedin's GW approximation is considered while quasiparticle calculations also improve estimates in the bandgap (Bechstedt *et al* 2009). Although it is possible to evaluate bulk modulus and cohesive energy from first-principles methods, estimates of these structural quantities are rarely reported for alloys than the binary compounds. A study on bandgap bowing and dielectric functions is reported on BeZnTe alloys by performing calculations using VASP package (Hafner 2008). In these calculations zinc atoms are replaced by beryllium in the *fcc* structure. The lattice parameters computed are found to follow the Vegaard's law (de Almeida and Ahuja 2006). In the alternative first-principles calculations for alloys, substitutional disorder is normally treated under the coherent-potential-approximation (Moroni and Jarlborg 1993; Saha *et al* 1994) but such studies are reported mostly for the binary transition metal alloys only.

[*]Author for correspondence (cmsmlsu@gmail.com)
[‡]Now at BARC, Mumbai

For the complex ternary, quaternary and pentanery semiconducting alloys the empirical pseudopotential method (EPM) within modified virtual crystal approximation (MVCA) is a good technique to explore the electronic structure (Cohen and Chelikowski 1988; Cohen 2006). EPM is one of the highly reliable and rapidly converging methods to study electronic band structure and relative properties of semiconductors. The structural alloying effects are modeled under the modified virtual crystal approximation (Bouarissa 2003) which has worked well for ternary and quaternary semiconductors (Swarnkar *et al* 2009; Joshi *et al* 2010). The computed band parameters can be used to quantify degree of covalence or ionicity.

In this work, we report electronic band structures, bandgaps, density of states (DOS), electronic charge densities of $Be_xZn_{1-x}Te$ alloys computed using the EPM. We also compute structural quantities like bulk modulus and cohesive energy. The computed band structure parameters are utilized to estimate ionicity. The electronic charge densities computed along a few planes are discussed with regard to the nature of bonding. Trends in ionicity are examined from charge density vis-à-vis ionicity factors computed on the basis of heteropolar gap (Al-Douri *et al* 2003).

2. Empirical pseudopotential method

EPM (Cohen and Chelikowski 1988; Al-Douri *et al* 2003; Swarnkar *et al* 2009; Joshi *et al* 2010) involves fitting of atomic form factors to the experimental data. The crystal potential $V(\mathbf{r})$ is then generated by superposition of atomic potentials

$$V(\mathbf{r}) = \sum_{\boldsymbol{R},\tau} V_{\mathrm{a}}(\mathbf{r} - \mathbf{R} - \tau), \tag{1}$$

where the summation extends over the lattice vector $\mathbf{R}$, basis vector $\boldsymbol{\tau}$, and the number of atoms in the primitive cell. In the reciprocal space the crystal potential can be written as

$$V(\mathbf{r}) = \sum_{\boldsymbol{G}} V_{\mathrm{a}}(\boldsymbol{G}) S(\boldsymbol{G})\, e^{i\mathbf{G}.\mathbf{r}}, \tag{2}$$

where $V_{\mathrm{a}}(\mathbf{G})$ is the form factor for the atomic potential and the structure factors $S(\mathbf{G})$ are given by

$$S(\mathbf{G}) = (1/N_{\mathrm{a}}) \sum_{\tau} e^{-iG.\tau}, \tag{3}$$

here N_{a} is the number of basis atoms. For zinc-blende structures if the origin is taken halfway between the two *fcc* lattices then $\tau = \pm(0{\cdot}125,\ 0{\cdot}125,\ 0{\cdot}125)a$ and for A^NB^{8-N} type compounds like BeTe and ZnTe, form factors can be simplified to

$$\boldsymbol{V}(\boldsymbol{G}) = \boldsymbol{V}^{\boldsymbol{S}}(\boldsymbol{G}) \cos(\boldsymbol{G}.\boldsymbol{\tau}) + i\boldsymbol{V}^{\boldsymbol{A}}(\mathbf{G}) \sin(\mathbf{G}.\boldsymbol{\tau}), \tag{4}$$

with $V^S(\mathbf{G}) = \frac{1}{2}[V_{\mathrm{A}}(\mathbf{G}) + V_{\mathrm{B}}(\mathbf{G})]$ and $V^A(\mathbf{G}) = \frac{1}{2}[V_{\mathrm{A}}(\mathbf{G}) - V_{\mathrm{B}}(\mathbf{G})]$.

The $V^{\mathrm{S}}(\mathbf{G})$ and $V^{\mathrm{A}}(\mathbf{G})$ are symmetric and anti-symmetric form factors, respectively. The pseudo wavefunction $\Psi_{n,\mathbf{k}}(\mathbf{r})$ is then a solution of the Schrodinger equation with the potential $V(\mathbf{r})$. In the local EPM the $\Psi_{n,\mathbf{k}}(\mathbf{r})$ is given by

$$\Psi_{n,\boldsymbol{k}}(\mathbf{r}) = \sqrt{\frac{1}{\Omega}} \sum_{\mathbf{G}} C_{n,\boldsymbol{k}}(\mathbf{G})\, e^{i(\mathbf{k}+\mathbf{G}).\mathbf{r}}, \tag{5}$$

where $C_{n,\mathbf{k}}(\mathbf{G})$ is the coefficient of the plane wave for a given reciprocal vector $\mathbf{G}$ and Ω the volume of the unit cell. The charge density can be calculated as

$$\rho_{\boldsymbol{k}}(\mathbf{r}) = \sum_{n} \left|\Psi_{n,\boldsymbol{k}}(\mathbf{r})\right|^2. \tag{6}$$

The charge density calculated over a dense grid of points can then be used to evaluate the total charge density. To compute band structure and charge density for the alloys, virtual crystal approximation (VCA) may be applied. Unlike metallic alloys the approximation has worked reasonably well to examine bandgaps, effective masses and bowing in other III–V and II–VI ternary and multi-component semiconductor alloys (Long *et al* 1996; Bechiri *et al* 2002; Bouarissa 2003; Ben Fredj *et al* 2007; Patel and Joshi 2007). However, for better description, effect of disorder needs to be considered. Therefore, we have used MVCA (Bechiri *et al* 2002; Ben Fredj *et al* 2007), which has shown improvement in the evaluation of bandgaps, effective masses and bowing in other III–V and II–VI ternary and multi-component semiconductor alloys (Bechiri *et al* 2002; Ben Fredj *et al* 2007; Swarnkar *et al* 2009; Joshi *et al* 2010). The lattice constants to compute the electronic band structure and charge densities for the ternary alloys are determined from Vegard's (1921) law which has been found to show consistent results for our system (de Almeida and Ahuja 2006). In MVCA, the alloying potential including the disorder effects for a ternary alloy is generated as

$$\begin{aligned} V^{S,A}_{\mathrm{Be}_x\mathrm{Zn}_{1-x}\mathrm{Te}} &= x V^{S,A}_{\mathrm{BeTe}} + (1-x) V^{S,A}_{\mathrm{ZnTe}} \\ &\quad - p\sqrt{x(1-x)} \left(V^{S,A}_{\mathrm{BeTe}} - V^{S,A}_{\mathrm{ZnTe}}\right). \end{aligned} \tag{7}$$

The disorder parameter, p, was adjusted to 0·495. These are derived by fitting the bandgaps at a number of symmetry points in the binary compounds. The lattice constants were taken from the X-ray measurements (Paszkowicz *et al* 2002) and 350 plane waves were used for the calculations.

Although it is possible to compute bulk modulus and cohesive energy from first-principles methods which require atomic numbers and crystal structures as input, alternative semi-empirical relations have been suggested by Philips (1973) and Cohen (1985) which have precision at par with the first-principles calculations (Cohen 2006). These relations are based on the idea that charge transfer decreases the covalent part of a heteropolar gap in IV, III–V and II–VI diamond and zinc-blende semicondutors. Following the

prescription of Cohen (1985, 2006), B_0(GPa) can be determined from the semi-empirical relation

$$B_0 = \frac{\langle N_c \rangle}{4} \frac{1531}{d^{7/2}}, \tag{8}$$

here $\langle N_c \rangle$ is the average coordination number and d the bond length in Ångstrom. Recently, Verma *et al* (2010) proposed a scheme to compute cohesive energy for III–V and II–VI zinc-blende compound semiconductors. We use their findings to propose cohesive energy for the alloys considered in this work.

3. Results and discussion

3.1 *Electronic band structure and density of states*

The electronic band structures and DOS of $Be_xZn_{1-x}Te$ alloys for the $x = 0{\cdot}2$, $0{\cdot}27$, $0{\cdot}4$, $0{\cdot}48$, $0{\cdot}6$ and $0{\cdot}8$ compositions have been computed. The alloy corresponding to $x = 0{\cdot}27$ shows crossover in the bandgap and the alloy with $x = 0{\cdot}48$ has lattice match with InP. Therefore, we give pictorial band structure and DOS for alloys with $x = 0{\cdot}27$ and $0{\cdot}48$. The salient features of band structures of other alloys are presented in table 1.

The band structures for binary end materials are reported earlier (Joshi *et al* 2009) which have shown that BeTe has an indirect bandgap of 2·81 eV along the Γ–X direction, whereas ZnTe has a direct bandgap of 2·26 eV. For all alloys reported here, the valence band maximum (VBM) is found at the Γ point. However, the conduction band minimum (CBM) shifts from Γ to X point of symmetry at $x = 0{\cdot}27$. In figure 1, we give band structure of $Be_{0{\cdot}27}Zn_{0{\cdot}73}Te$ alloy. The bands are designated as per the standard definitions used by Bernard and Zunger (1986, 1987). The DOS are plotted on the right panel of the figure. It is visually obvious that the observed bandgap is 2·61 eV which is well in accordance with the experimental observations reported by Maksimov and Tamargo (2001) who observed a crossover at $x = 0{\cdot}28$ with a 2·77 eV bandgap. In figure 2, we give the electronic band structure and DOS for the $Be_{0{\cdot}48}Zn_{0{\cdot}52}Te$ alloy having lattice match with the InP. It depicts that the alloy has Γ–X gap of 2·48 eV and Γ–Γ gap of 4·14 eV against the experimentally observed 2·77 eV and 3·14 eV, respectively. The Γ–X and Γ–Γ gaps for InP are 1·42 eV and 2·38 eV, respectively (Vurgaftman *et al* 2001). Considering the fact that GW calculations (Nagelstraβer *et al* 1998) also underestimate (2·6 eV) the bandgap in BeTe, our results on alloys may be useful in further studies.

The typical DOS for the $Be_{0{\cdot}27}Zn_{0{\cdot}73}Te$ and $Be_{0{\cdot}48}Zn_{0{\cdot}52}Te$ alloys are plotted on the right panels of figures 1 and 2, respectively. It is obvious that overall topology of the occupied DOS is similar. However, the unoccupied DOS within 2·77–4·5 eV shows subtle differences. For the alloy with $x = 0{\cdot}27$, a few peaks appear while in $x = 0{\cdot}48$ alloy these are missing. Also DOS at the upper energy level (5·5 eV)

Table 1. Characteristics of electronic band structures of $Be_xZn_{1-x}Te$ alloys. The bandwidth of upper three valence bands (UVB) and total valence bandwidth (TVB) are also given.

Alloy		Bandgap, E_g (eV)				Bandwidths (eV)		
		Γ–Γ	Γ–X	Γ–L	$X_c^1 - X_c^3$	UVB	TVB	f_i
ZnTe	This work	2·26	3·06	3·50	1·50	3·32	11·45	0·651
	Theory[a]	1·32	2·17					0·546[b], 0·684[c]
	Expt.[d]	2·26	3·06					
$Be_{0{\cdot}2}Zn_{0{\cdot}8}Te$	This work	2·28	2·69	3·42	1·73	3·68	11·55	0·638
	Expt.[d]	2·63	2·92					
$Be_{0{\cdot}27}Zn_{0{\cdot}73}Te$	This work	2·61	2·61	3·53	1·73	3·82	11·36	0·621
	Expt.[d]	2·76	2·88					
$Be_{0{\cdot}4}Zn_{0{\cdot}6}Te$	This work	3·47	2·51	3·84	1·66	4·09	11·02	0·580
	Expt.[d]	3·00	2·83					
$Be_{0{\cdot}48}Zn_{0{\cdot}52}Te$	This work	4·14	2·48	4·07	1·58	5·54	10·83	0·549
	Expt.[d]	3·14	2·81					
InP	Expt.[e]	1·42	2·38	2·01				
$Be_{0{\cdot}6}Zn_{0{\cdot}6}Te$	This work	4·96	2·47	4·44	1·42			0·494
	Expt.[d]	3·37	2·78					
$Be_{0{\cdot}8}Zn_{0{\cdot}2}Te$	This work	4·55	2·53	4·06	1·06	3·77	10·40	0·379
	Expt.[d]	3·73	2·77					
BeTe	This work	4·15	2·81	3·76	0·44	5·14	10·26	0·219
	Theory[f]	3·6	1·8					0·17[b]
	Expt.[d]	4·10	2·8					

[a]Chen *et al* (1996); [b] Philips (1973); [c]Zaoui *et al* (1994); [d]Maksimov and Tamargo (2001); [e]Vurgaftman *et al* (2001); [f]Gonzalez-Diaz *et al* (1997).

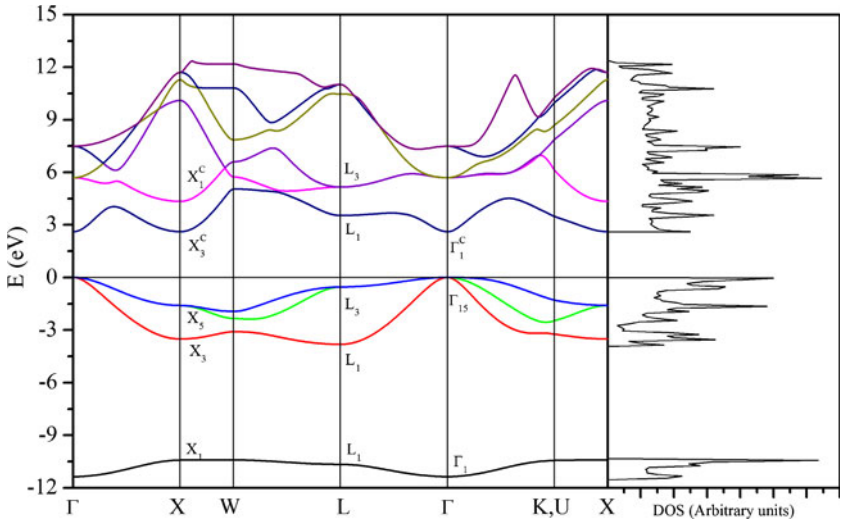

Figure 1. Band structure of $Be_{0.27}Zn_{0.73}Te$ alloy. Band symbols are taken from Bernard and Zunger (1986, 1987). Panel on right hand shows the total density of states.

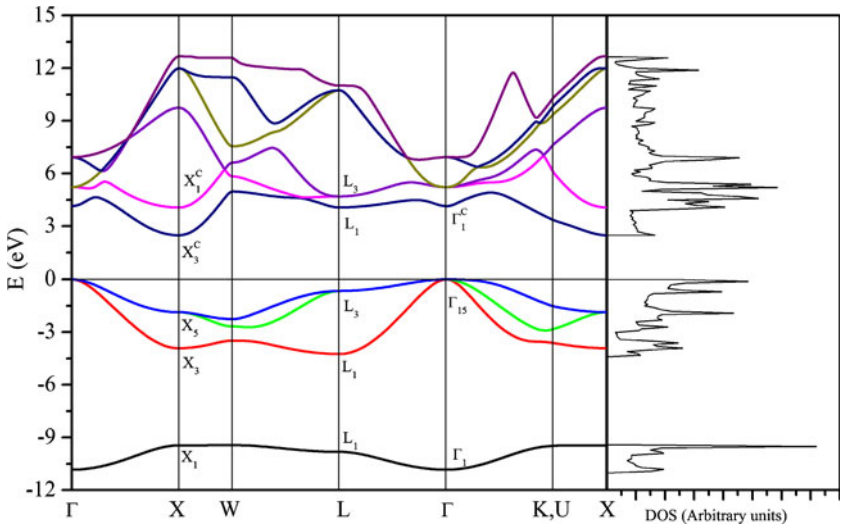

Figure 2. Band structure of $Be_{0.48}Zn_{0.52}Te$ alloy. Panel on right hand shows the total density of states.

rises. As first two conduction bands contribute mainly to the DOS in this region it may probably be a bonding effect on the first two conduction bands resulting from alloying. For instance, the two lowest conduction bands come closer at the X-point as the alloy becomes Be rich. Such behaviour is seen in other alloys also (see separation in X states in table 1 for other alloys). It may be a consequence of covalent character of bonding in Be rich alloy which will be discussed with subsequent findings.

In table 1, we give salient features of the band structures of all alloys studied in this work. The results are in reasonable agreement with the measurements. Knowing that Maksimov and Tamargo (2001) performed measurements on the epilayers at room temperature and subtle stoichiometric uncertainties remaining in the samples, our results may be taken to be in very good agreement. It is well known for zinc chalcogenides that in the $X^c_{1,3}$ states charge is between the constituents. In the X^c_1 state charge is between anions and in the X^c_3, charge is between cations (Bernard and Zunger 1986, 1987). Consequently, effect of cationic substitution (Be,Zn) may probably result in separation between X^c_1 and X^c_3 conducting bands (Bernard and Zunger 1986). Striking feature compared to the first-principles calculations on ZnTe (Bernard and Zunger 1987) is separation in the X^c_1 and X^c_3

conducting bands which continues till W in figures 1 and 2. It may be noted that X_c^1 and X_c^3 states show larger gap of 1·5 eV in ZnTe compared to 0·44 eV in BeTe. The substitution effects are clearly visible on the $X_{1,3}^c$ states depicted in band structures of the alloys plotted in figures 1 and 2. The separation is 1·73 eV, 1·55 eV and 1·16 eV for $Be_{0.25}Zn_{0.75}Te$, $Be_{0.50}Zn_{0.50}Te$ and $Be_{0.75}Zn_{0.25}Te$ alloys, respectively. For other alloys, listed in table 1, separation between X_1^c and X_3^c conducting bands decreases on increasing content of beryllium. As observed for the end materials, it points to a higher covalent bonding character in beryllium rich alloys. It is also reflected as increase in the bandwidths of the upper three valence bands listed in table 1. To quantify the degree of covalent or ionic character, the ionicity factor f_i is computed following the formulation of Al-Douri *et al* (2003). The computed ionicity factor f_i, listed in table 1, clearly shows that beryllium rich alloys have more covalent character.

Now we discuss bowing in the energy gaps. In figure 3, we have plotted energy gaps at the Γ, X and L points of symmetry considering the MVCA. To generate these curves we have performed calculations for additional nine compositions. The E_Γ and E_L increase until $x = 0{\cdot}6$ and decreases thereafter. Beyond $x = 0{\cdot}6$, identical composition dependent trend in the energy gaps is clearly visible. A striking feature is the observation of Γ–X crossover that is marked by a pointer in the figure. The MVCA shows Γ–X crossover at $x = 0{\cdot}27$. This is well in accordance with the experimentally reported composition $x = 0{\cdot}28$ (Maksimov and Tamargo 2001). The first-principles calculations have shown it to occur at $x = 0{\cdot}20$ on the basis of five compositions including end compounds against fourteen compositions studied by us (de Almeida and Ahuja 2006). The well-known

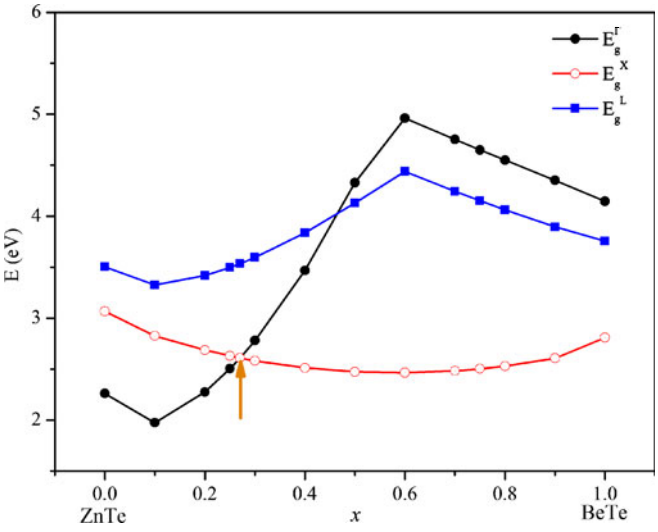

Figure 3. Variation of bandgaps at various points of symmetry with concentration of Be. The points show calculated gaps and the lines are drawn to guide eye scan.

underestimation of bandgaps by first-principles calculations may probably be one of the reasons for this discrepancy (Bechstedt *et al* 2009).

It has been recognized that three effects contribute to the origin of bowing in semiconducting alloys, i.e. volume deformation (VD), charge exchange (CE) and the structural relaxation (SR) effects (Ferhat and Bechstedt 2002). The VD effect accounts for the effect on band structures arising from the change of equilibrium lattice constants. This factor will have larger contribution in the alloys tailored from the binary compounds having larger lattice mismatch. The CE effect ascribes the effect on band structure arising from the electronegativity mismatch without considering sublattice relaxation. The SR effect is weak having very small impact on the bowing of alloys. In the BeZnTe alloys, figure 3 shows larger nonlinear effect and hence bowing. The lattice and the electronegativity mismatch (Martienssen and Warlimont 2005) in cations for BeZnTe alloys are 8% and 11%, respectively. The SR effect is negligibly smaller as Vegaards law is used. Thus, bowing is mainly due to VD and CE effects. As these effects are considered in the MVCA through disorder parameter, it gives better results than the VCA. However, more such studies will aptly justify application of MVCA for ternary and quaternary semiconductor alloys.

3.2 *Structural properties*

As mentioned earlier, owing to the complexities involved, it is difficult to perform first-principles calculations for the ternary and quaternary alloys. Only recently, a few calculations have appeared but none of these reported structural parameters viz. bulk modulus, cohesive energy etc. (de Almeida and Ahuja 2006; Hassan *et al* 2006; Boukortt *et al* 2010). It is worthy to note that we have calculated structural quantities following Vegard's law which presumes perfectly rigid lattice for the alloys. The first-principle calculations (de Almeida and Ahuja 2006) have shown that BeZnTe alloys follow Vegard's law and so rigid lattice model may be valid to compute the structural quantities for these alloys. Therefore, we provide the bulk modulus for the BeZnTe alloys including binary end materials using (8) and cohesive energy following the prescription of Verma *et al* (2010). The quantities obtained are listed in table 2. One can infer that for binary compounds our results are in very good agreement and therefore, structural parameters for other alloys may be very useful and relevant for further studies. The availability of experimental data will be useful to examine these results and model critically.

3.3 *Charge density*

Although we have computed charge density along a number of planes for all compositions, we present results of only a few compositions here. The various planes considered for the zinc-blende structure of alloys are shown in figure 4. We

Table 2. Structural parameters for $Be_xZn_{1-x}Te$ alloys.

Alloy		B_0(GPa)	E_{coh}(eV)
ZnTe	Expt.	51·0[a]	4·61[b]
	Theory	51·2[a]	4·71[b]
	This work	51·0	4·72
$Be_{0.2}Zn_{0.8}Te$	This work	53·91	4·91
$Be_{0.27}Zn_{0.73}Te$	This work	54·98	4·98
$Be_{0.4}Zn_{0.6}Te$	This work	57·03	5·11
$Be_{0.48}Zn_{0.52}Te$	This work	58·34	5·19
$Be_{0.6}Zn_{0.8}Te$	This work	60·38	5·32
$Be_{0.8}Zn_{0.2}Te$	This work	63·99	5·55
BeTe	Expt.	67·0[c]	–
	Theory	60·0[d]	–
	This work	67·88	5·79

[a]Cohen (2006); [b]Verma *et al* (2010); [c]Luo *et al* (1995); [d]Srivastava *et al* (2004).

focus our discussion on the charge density calculations performed at $\Gamma = 0$ point for BeTe, $Be_{0.48}Zn_{0.52}Te$ and ZnTe. The overall topology and nature of charge density distribution can be interpreted on the basis of atomic positions in the $z = 0{\cdot}0$, $0{\cdot}125$ and $0{\cdot}25$ planes shown in figure 4. In figures 5(a)–(c), we plot charge density in the cation plane, i.e. $z = 0{\cdot}0$. In this plane charge is more delocalized for BeTe (figure 5(a)) and localization increases gradually as the alloy becomes Zn rich. The charge density obtained for the $Be_{0.48}Zn_{0.52}Te$ alloy along $z = 0{\cdot}125$ and $z = 0{\cdot}25$ are shown in figures 6(a) and (b), respectively. A close inspection of figures 5(b), 6(a) and 6(b) for $Be_{0.48}Zn_{0.52}Te$ reveals that charge distribution is more intense half-way along the diagonal in the bond intersecting plane ($z = 0{\cdot}125$). Also, the charge distribution is more intense compared to the anion plane ($z = 0{\cdot}25$). Moreover, the charge density around atomic positions in the anion plane is lower compared to the cation plane. It has been observed from calculations on other compositions that charge density in the bond intersecting plane is

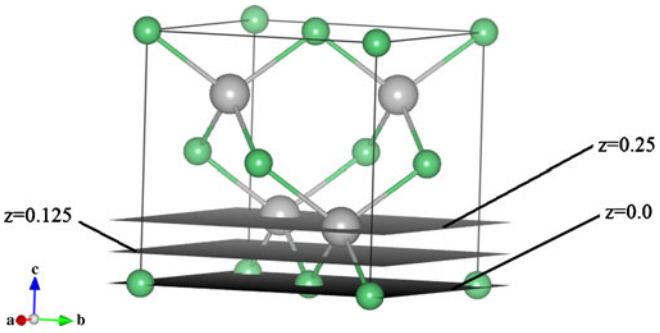

Figure 4. Zinc-blende structure of the $Be_xZn_{1-x}Te$ alloys. The cation plane $z = 0{\cdot}0$, bond intersecting plane $z = 0{\cdot}125$ and the anion plane $z = 0{\cdot}25$ used to compute charge density are shaded.

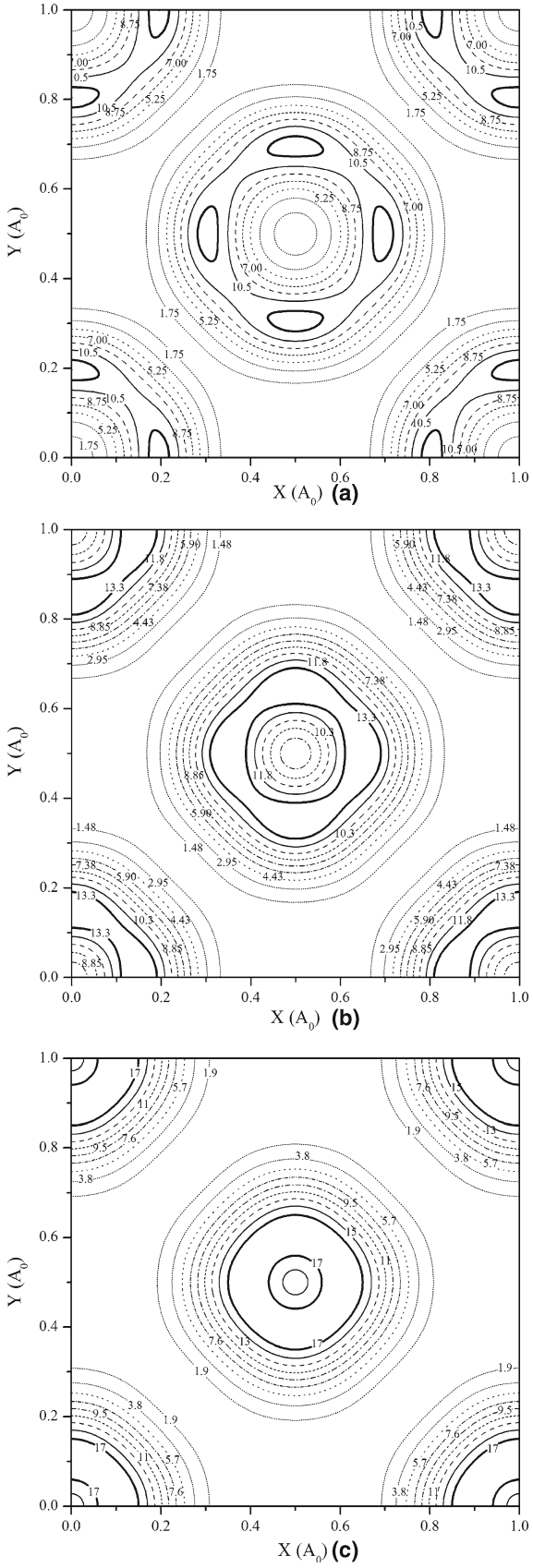

Figure 5. Charge density obtained at the gamma point along the $z = 0{\cdot}0$ plane for (**a**) BeTe, (**b**) $Be_{0.48}Zn_{0.52}Te$ and (**c**) ZnTe.

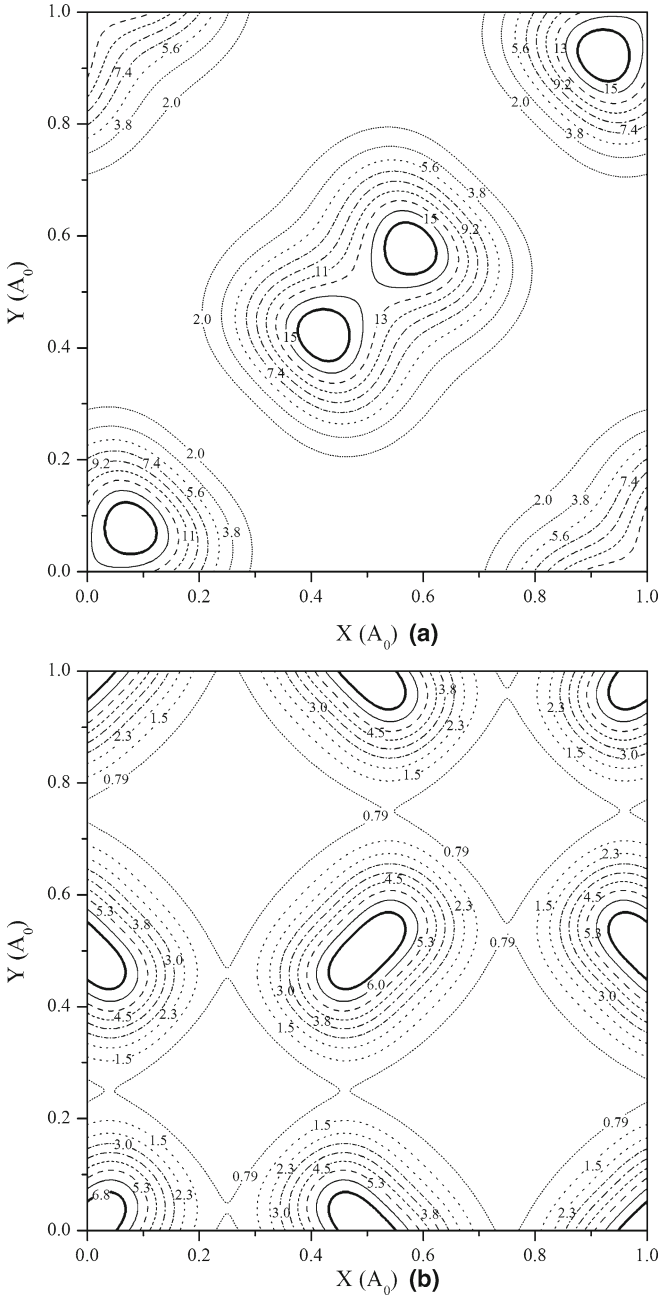

Figure 6. Charge density obtained at the gamma point for $Be_{0.48}Zn_{0.52}Te$ alloy along (**a**) bond intersecting plane $z = 0{\cdot}125$ and (**b**) anion plane $z = 0{\cdot}25$.

more in Be rich alloys. It indicates covalent nature of bonding in Be rich alloys as suggested by the ionicity factors listed in table 1.

4. Conclusions

Electronic structure for $Be_xZn_{1-x}Te$ alloys are studied using EPM under the modified virtual crystal approximation. The electronic band structure calculations obtained under the regime of MVCA show direct to indirect crossover in $Be_{0.27}Zn_{0.73}Te$ alloy. Our results are closer to the experimental findings. On the basis of separation between X_1^C and X_3^C states, ionicity, and charge density distribution, higher covalent character of bonding is found in the Be rich alloys. In the cation plane charge is more delocalized in BeTe and localization increases gradually as the alloy becomes Zn rich.

Acknowledgements

One of the authors (UP) is grateful to CSIR, New Delhi, for awarding a JRF. The financial support by DST, New Delhi, is gratefully acknowledged.

References

Adachi S 2009 *Properties of semiconductor alloys group IV, III–V and II–VI semiconductors* (West Sussex, UK: John Wiley & Sons Ltd.)

Al-Douri Y, Khenata R, Chikr Z C, Driz M and Aourag H 2003 *J. Appl. Phys.* **94** 4502

Bechiri A, Benmakhlouf F and Bouarissa N 2002 *Mater. Chem. Phys.* **77** 507

Bechstedt F, Fuchs F and Kresse G 2009 *Phys. Status Solidi (b)* **246** 1877

Ben Fredj A, Debbichi M and Said M 2007 *Microelectron. J.* **38** 860

Berghout A, Zaoui A, Hugel J and Ferhat M 2007 *Phys. Rev.* **B75** 205112

Bernard J E and Zunger A 1986 *Phys. Rev.* **B34** 5992

Bernard J E and Zunger A 1987 *Phys. Rev.* **B36** 3199

Bouarissa N 2003 *Eur. Phys. J.* **B32** 421

Boukortt A, Berrah S, Hayn R and Zaoui A 2010 *Physica* **B405** 763

Che S B, Nomura I, Kikuchi A and Kishino K 2002 *Appl. Phys. Lett.* **81** 972

Chen X, Hua X, Hu J, Langlois J M and Goddard W A 1996 *Phys. Rev.* **B53** 1377

Cohen M L 1985 *Phys. Rev.* **B32** 7988

Cohen M L 2006 *Annu. Rev. Mater. Sci.* **30** 1

Cohen M L and Chelikowski J R 1988 *Electronic structure and optical properties of semiconductors* (Berlin: Springer-Verlag) Vol. 75

de Almeida J S and Ahuja R 2006 *Appl. Phys. Lett.* **89** 61913

Dhamani R, Riba L S, Beesabathina D P, Nguyen N V, Horowitz D C and Jonker B T 1993 *Evolution of surface and thin film microstructure symposium, Proceedings materials research society* (eds) H A Atwater *et al* (Pitsburg, PA: MRS)

Fan Y *et al* 1992 *Appl. Phys. Lett.* **61** 3160

Ferhat M and Bechstedt F 2002 *Phys. Rev.* **B65** 75213

Gonzalez-Diaz M, Rodriguez-Hernandez P and Munoz A 1997 *Phys. Rev.* **B55** 14043

Hafner J 2008 *J. Comput. Chem.* **29** 2044

Hassan F E H, Hashemifar S J and Akbarzadeh H 2006 *Phys. Rev.* **B73** 195202

Joshi K B, Pandya R K, Kothari R K and Sharma B K 2009 *Phys. Status Solidi (b)* **246** 1268

Joshi K B, Patel N N, Swarnkar C B and Paliwal U 2010 *Comp. Mater. Sci.* **49** S246

Kalpana G, Pari G, Mookerjee A and Bhattacharya A K 1998 *Int. J. Mod. Phys.* **B12** 1975
Kishino K and Nomura I 2002 *IEEE-J. Sel. Top. Qaunt. Electr.* **8** 773
Long F, Harrison P and Hagston W E 1996 *J. Appl. Phys.* **79** 6939
Luo H, Ghandehari K, Greene R G, Ruoff A L, Trail S S and DiSalvo F J 1995 *Phys. Rev.* **B52** 7058
Maksimov O and Tamargo M C 2001 *Appl. Phys. Lett.* **79** 782
Maksimov O, Munoz M, Samarth N and Tamargo M C 2004 *Thin Solid Films* **467** 88
Martienssen W and Warlimont H 2005 *Handbook of condensed matter and materials data* (Berlin: Springer)
Moroni E G and Jarlborg T 1993 *Phys. Rev.* **B47** 3255
Nagelstraβer M *et al* 1998 *Phys. Rev.* **B58** 10394
Nakamura S, Senoh M, Nagahama S, Iwasa N, Matsushita T and Mukai T 2000 *Appl. Phys. Lett.* **76** 22
Niiyama Y and Watanabe M 2005 *Semicond. Sci. Technol.* **20** 1187
Paszkowicz W, Firszt F, Legowski S, Meczynska H, Zakrzewski J and Marczak M 2002 *Phys. Status Solidi (b)* **229** 57
Patel N N and Joshi K B 2007 *Eur. Phys. J.* **B59** 19
Philips J C 1973 *Bonds and bands in semiconductors* (New York: Academic)
Saha T, Dasgupta I and Mookerjee A 1994 *J. Phys.: Condens. Matter* **6** L245
Srivastava G P, Tutuncu H M and Gunhan N 2004 *Phys. Rev.* **B70** 85206
Stukel D J 1970 *Phys. Rev.* **B2** 1852
Swarnkar C B, Pandya R K, Paliwal U, Patel N N and Joshi K B 2009 *Chalco. Lett.* **6** 137
Vegard L 1921 *Z. Phys.* **5** 17
Verie C 1995 *Semiconductors heteroepitaxy* (eds) B Gil and R L Aulombard (Singapore: World Scientific) p 73
Verie C 1997 *Mater. Sci. Eng.* **B43** 60
Verma A S, Sarkar B K and Jindal V K 2010 *Pramana–J. Phys.* **74** 851
Vurgaftman I, Meyer J R and Ram-Mohan L R 2001 *J. Appl. Phys.* **89** 5815
Waag A et al 1996 *J. Appl. Phys.* **80** 792
Waag A et al 1997 *Appl. Phys. Lett.* **70** 280
Zaoui A, Ferhat M, Khelifa B, Dufour J P and Aourag H 1994 *Phys. Status Solidi (b)* **185** 163